Robo2 contains a cryptic binding site for neural EGFL-like (NELL) protein 1/2

Received for publication, September 13, 2018, and in revised form, January 14, 2019 Published, Papers in Press, January 30, 2019, DOI 10.1074/jbc.RA118.005819

Naoka Yamamoto[‡], Manabu Kashiwagi[‡], Manami Ishihara[‡], Takaaki Kojima[‡], Andrés D. Maturana[‡], Shun'ichi Kuroda[§], and Tomoaki Niimi[‡1]

From the [‡]Graduate School of Bioagricultural Sciences, Nagoya University, Nagoya 464-8601, Japan and the [§]Institute of Scientific and Industrial Research, Osaka University, Osaka 567-0047, Japan

Edited by Luke O'Neill

The signaling pathways that are mediated by Slit ligands and their Roundabout (Robo) family of receptors play multifunctional roles in the development of the nervous system and other organs. A recent study identified neural epidermal growth factor–like (NEL)–like 2 (NELL2) as a novel ligand for Robo3. In this study, we carried out a comprehensive analysis of the interaction between NELL1 and the Robo family of receptors and demonstrated that Robo2 contains a cryptic binding site for both NELL1 and NELL2. NELL1/2 binds to the first fibronectin type III (FNIII) domain of Robo2 but not to intact Robo2. Mutation analysis revealed that several amino acids within the first FNIII domain are critical for NELL1 binding to Robo2 but not to Robo1. The Robo2 deletion mutants without the fourth immunoglobulin domain and single amino acid substitution mutants that can influence the architecture of the ectodomain facilitated binding to NELL1/2. Acidic conditions increased the binding affinity of Robo2 for NELL1. These results suggest that Robo2 functions as a receptor for NELL1/2, particularly under circumstances where Robo2 undergoes proteolytic digestion. If this is not the case, conformational changes of the ectodomain of Robo2 may unmask the binding site for NELL1/2.

Neural epidermal growth factor-like (EGFL)-like[2] 1 (NELL1) and NELL2 constitute a family of large secretory glycoproteins that contain a laminin G domain, four von Willebrand factor type C domains, and six EGFL repeats (1, 2). Both proteins are expressed primarily in developing and adult brain. NELL2 plays multiple roles in neuronal development, survival, and activity (3, 4), whereas NELL1 functions as a regulator of craniofacial skeletal morphogenesis (5). The *NELL1* gene was originally identified as a gene overexpressed in human sporadic coronal craniosynostosis (6). Transgenic mice overexpressing NELL1 display a phenotype similar to human craniosynostosis patients, which is characterized by premature cranial suture closure with bone overgrowth, whereas *NELL1*-deficient mice have cranial and vertebral skeletal defects (7–9). NELL1 has been shown to induce osteogenic differentiation partially through the integrin β1 receptor following activation of mitogen-activated protein kinase and canonical Wnt signaling pathways (10–12). Recent studies suggest that NELL1 also plays a role in chondrogenic differentiation and maturation through Indian hedgehog signaling (13–15). However, the molecular mechanism underlying NELL1-induced osteogenic and chondrogenic differentiation, especially specific receptors for NELL1, is not fully understood.

Roundabout (Robo) single-pass transmembrane receptors belongs to the Ig superfamily of cell adhesion molecules (16–18). In mammals, four members of Robo (Robo1–4) have been identified. The extracellular domain of Robo1–3 contains five Ig and three fibronectin type III (FNIII) domains, whereas Robo4 has only two Ig and two FNIII domains. Robo receptors and their Slit ligands (Slit1–3), which were originally identified as important axon guidance molecules, have also been shown to function in a number of developmental events outside the nervous system (19, 20). Recently, NELL2 was identified as a secreted ligand for Robo3, thereby functioning as a repulsive axon guidance cue that contributes to commissural axon guidance to the midline (21). Although Robo3 binds both NELL1 and NELL2, NELL1 has no effect on commissural axon repulsion. These findings raise questions as to why NELL1 and NELL2 have different effects on commissural axon guidance following interaction with Robo3 and whether Robo3 is an exclusive receptor for NELL1 among the Robo family of receptors.

In the present study, we carried out a comprehensive analysis of the interaction between NELL1 and the Robo family of receptors in both cell-free and cell-based binding assays. We found that the FNIII domains of Robo2 have strong binding activity to both NELL1 and NELL2. Robo2 binds to the second and the third EGFL repeats of NELL1 through its first FNIII domain, and the critical amino acids for NELL1 binding were identified within the FNIII domain. The Robo2 deletion mutants without the fourth Ig domain and under acidic conditions facilitated binding to NELL1/2. These results raise the

This work was supported by Japan Society for the Promotion of Science KAKENHI Grants 26350959 and 17K01946. The authors declare that they have no conflicts of interest with the contents of this article.

This article contains Figs. S1–S12.

[1] To whom correspondence should be addressed: Graduate School of Bioagricultural Sciences, Nagoya University, Furo-cho, Chikusa-ku, Nagoya 464-8601, Japan. Tel.: 81-52-789-5015; Fax: 81-52-789-5237; E-mail: tniimi@agr.nagoya-u.ac.jp.

[2] The abbreviations used are: EGFL, epidermal growth factor-like; ECD, extracellular domain; FNIII, fibronectin type III; NELL, neural epidermal growth factor–like (NEL)–like; Robo, Roundabout; HA, hemagglutinin; AP, alkaline phosphatase; BLI, biolayer interferometry; SEC, size-exclusion chromatography; BCIP, 5-bromo-4-chloro-3-indolyl-phosphate; NBT, nitroblue tetrazolium.

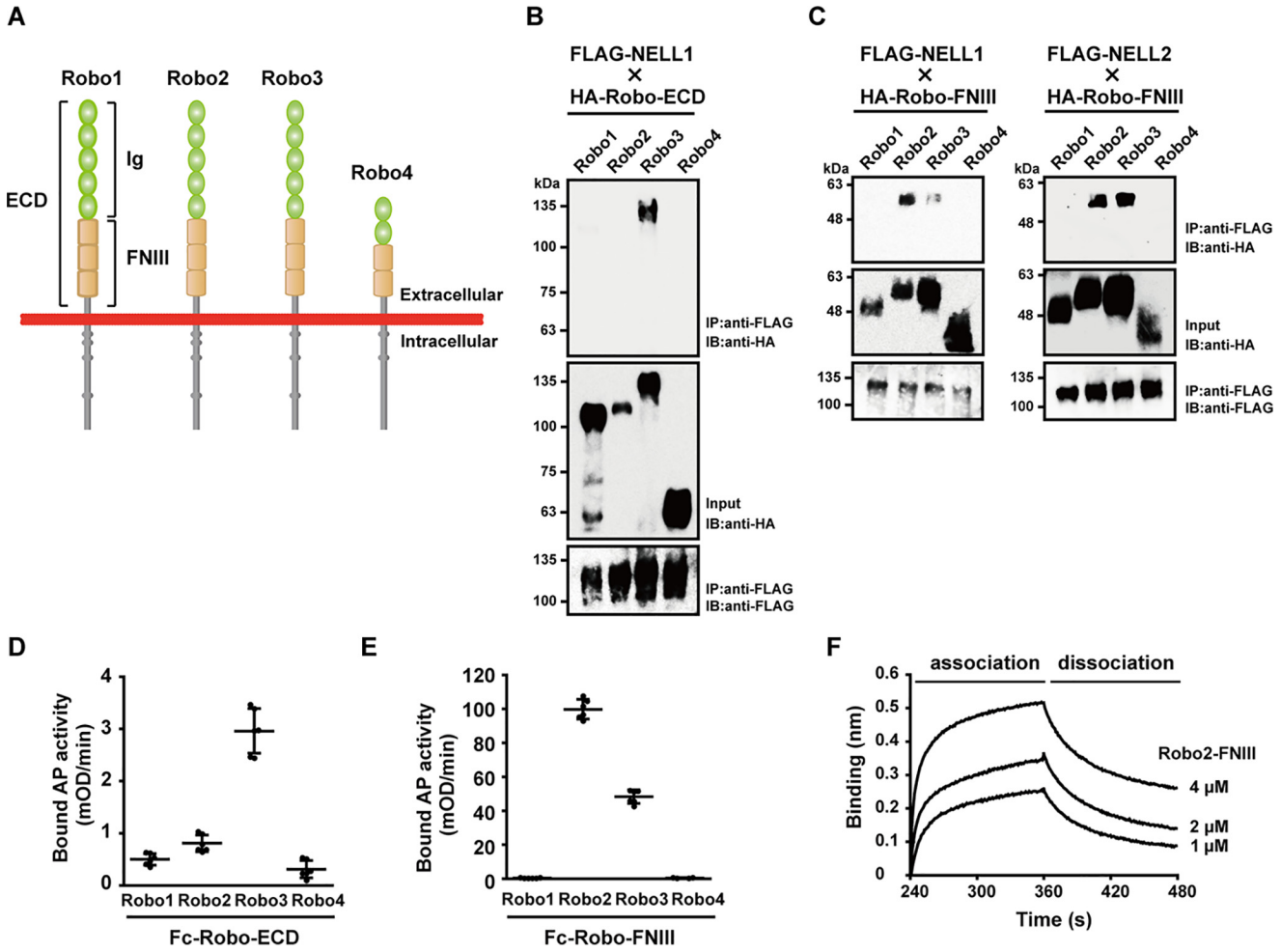

Figure 1. Interaction between NELL1/2 and Robo receptors. *A*, schematic diagrams of Robo receptors and their structural domains. *B* and *C*, interaction between NELL1/2 and Robo proteins in the solution-binding assay. Conditioned media of FLAG-tagged NELL1/2 and HA-tagged ECDs (*B*) or FNIII domains (*C*) of Robo1–4 were mixed and then incubated with anti-FLAG affinity beads. Bound proteins were isolated by immunoprecipitation, resolved by SDS-PAGE, and visualized by immunoblotting (*IB*) with the anti-HA antibody. *D* and *E*, interaction between NELL1 and Robo proteins in the solid-phase binding assay. Conditioned medium of Fc-tagged ECD (*D*) or FNIII domains (*E*) of Robo1–4 was allowed to bind to protein A–coated plates and then incubated with conditioned medium of AP-tagged NELL1. The bound AP activity was measured by adding the AP substrate. Each value represents the mean ± S.D. of triplicate results ($n = 6$). *F*, BLI analysis was performed to assess binding affinity between Robo2-FNIII and immobilized full-length NELL1. The BLI sensorgrams show the binding response of Robo2-FNIII at the indicated concentrations.

possibility that NELL1/2 interacts with Robo2, particularly under conditions where Robo2 undergoes proteolytic digestion or in an acidic environment.

Results

Interaction of NELL1/2 with the Robo family of receptors

To investigate whether NELL1 binds to proteins of the Robo family (Fig. 1*A*), we first performed binding assays in solution using FLAG-tagged NELL1 and the HA-tagged extracellular domain (ECD) of Robo1–4. As shown in Fig. 1*B*, Robo3-ECD co-immunoprecipitated with full-length NELL1, which is consistent with a previous report (21), but other Robo proteins did not co-immunoprecipitate with NELL1. Because NELL2 binds to FNIII domains of Robo3 (21), we next performed solution-binding assays using the FNIII domains of Robo1–4 instead of the ECD. Interestingly, NELL1 bound not only to the FNIII domain of Robo3 but also strongly to that of Robo2 (Fig. 1*C*, *left panel*). Similar results were obtained using FLAG-tagged NELL2 (Fig. 1*C*, *right panel*).

To confirm these results, solid-phase binding assays were performed using alkaline phosphatase (AP)–tagged NELL1 and Fc-tagged Robo1–4 in 96-well plates coated with protein A. AP-tagged NELL1, but not AP alone, bound to Fc-tagged Robo2-FNIII but not to Fc alone (Fig. S1). Further, AP-tagged NELL1 bound to Fc-Robo2 and -Robo3 in a similar manner to that observed in the solution-binding assays (Fig. 1, *D* and *E*, and Fig. S2).

We performed cell-free binding assays using purified proteins to exclude the possibility that these results were because of indirect interactions mediated by other proteins present in conditioned media (Fig. S3). In the solid-phase binding assay, we used AP-tagged NELL1 containing only the C-terminal region because a sufficient amount of AP-tagged full-length NELL1 was not obtained because of a low expression level. Nevertheless, these assays demonstrated that NELL1 interacts with the FNIII domain of both Robo2 and Robo3.

We also confirmed the interaction between NELL1 and the FNIII domain of Robo2 by biolayer interferometry (BLI)

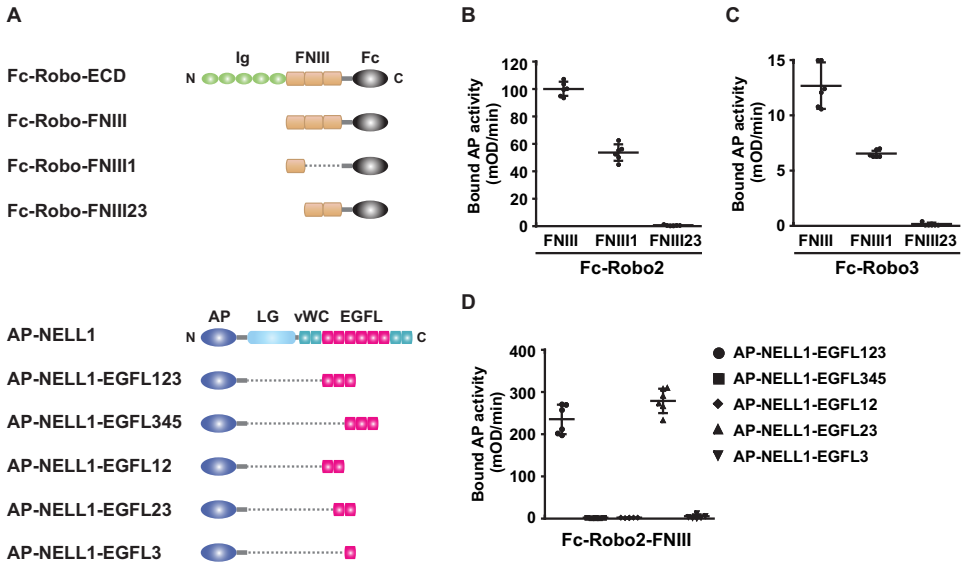

Figure 2. Identification of binding domains between NELL1 and Robo2. *A*, schematic diagrams of the Fc-tagged Robo and the AP-tagged NELL1 fragments. *B* and *C*, conditioned medium of Fc-tagged Robo2 (*B*) or Robo3 (*C*) fragments containing either all three, two, or one of the FNIII domains was allowed to bind to protein A–coated plates and then incubated with conditioned medium of AP-tagged NELL1. The bound AP activity was measured by adding the AP substrate. Each value represents the mean ± S.D. of triplicate results ($n = 6$). *D*, conditioned medium of Fc-tagged Robo2-FNIII domains was allowed to bind to protein A–coated plates and then incubated with conditioned medium of AP-tagged NELL1 fragments containing either three, two, or one of the EGFL repeats. The bound AP activity was measured as above. *vWC*, von Willebrand factor type C domain

analysis (Fig. 1*F* and Fig. S4). These results suggested that Robo2 contains a cryptic binding site for NELL1/2 in FNIII domains.

Robo2 interacts with the EGFL repeats of NELL1 through the first FNIII domain

To determine which domain of Robo2 interacts with NELL1, deletion mutants of Fc-tagged Robo2-FNIII were prepared, and the binding activity was examined. The first FNIII domain (FNIII1) bound to NELL1, whereas the construct consisting of the second and third FNIII domains (FNIII23) did not bind, suggesting that Robo2 interacts with NELL1 through the first FNIII domain (Fig. 2, *A* and *B*, and Fig. S5). Similar results were obtained using the deletion mutants of Fc-tagged Robo3-FNIII (Fig. 2*C*).

Conversely, to determine which domain of NELL1 interacts with Robo2, deletion mutants of AP-tagged NELL1 EGFL domains were prepared because NELL2 binds to Robo3 through the EGFL domains (21). Although the construct containing all six EGFL domains and constructs containing the sixth EGFL domain could not be examined because of difficulties with recombinant production, the construct consisting of the first three EGFL domains (EGFL123) was observed to interact with Robo2-FNIII, whereas the construct composed of EGFL domains three to five (EGFL345) did not bind (Fig. 2, *A* and *D*, and Fig. S5). Further, the construct consisting of the second and third EGFL domains (EGFL23) bound to Robo2-FNIII, whereas the construct consisting of the first and second EGFL domains (EGFL12) and the construct composed of the third EGFL domains (EGFL3) did not show binding, indicating that both the second and the third EGFL domains are required for interaction between NELL1 and Robo2.

Identification of critical amino acids in the first FNIII domain of Robo2 for NELL1 binding

Amino acid sequence alignment of the first FNIII domain and linker region of mouse and human Robo1–3 shows very high homology among Robo members (51–61% identity and 71–80% similarity) (Fig. 3*A*), which enabled identification of potentially critical amino acids for NELL1 binding. Because NELL1 binds to the first FNIII domain of both Robo2 and Robo3, we focused on identifying amino acid residues that only differ between Robo1 and Robo2/3. Eight residues were found in the FNIII1 domain (Fig. 3*A*); however, we ignored Ser^{523} residue of mRobo1 (Gly^{523} of mRobo2) because it is located on the border of this domain. To investigate whether the remaining seven amino acid residues are involved in NELL1 binding, we prepared a series of mutant constructs of Fc-Robo2-FNIII in which the corresponding residues were substituted with those of Robo1 and tested the NELL1-binding activity of these mutants (Fig. 3*B* and Fig. S6). Because Var^{564} and Asn^{566} of mRobo2 are located close to each other, we prepared one construct with a double mutation (V564S and N566S). Among the five single mutants examined, the T581A mutant exhibited significant loss of NELL1-binding activity. Furthermore, a double or triple mutant containing the T581A mutation, such as T581A/T589A or V564S/N566S/T581A, showed complete loss of NELL1-binding activity. These results indicate that Thr^{581} plays a central role in NELL1 binding. A double mutant without the T581A mutation (T589A/P608Q) also exhibited significant loss of NELL1-binding activity, suggesting that several amino acids including Thr^{581} are responsible for NELL1 binding.

We next prepared a series of mutant constructs of Fc-Robo1-FNIII where the corresponding residues were substituted with those of Robo2 and tested the NELL1-binding activity of these mutants (Fig. 3*C* and Fig. S6). Although a single mutant with the

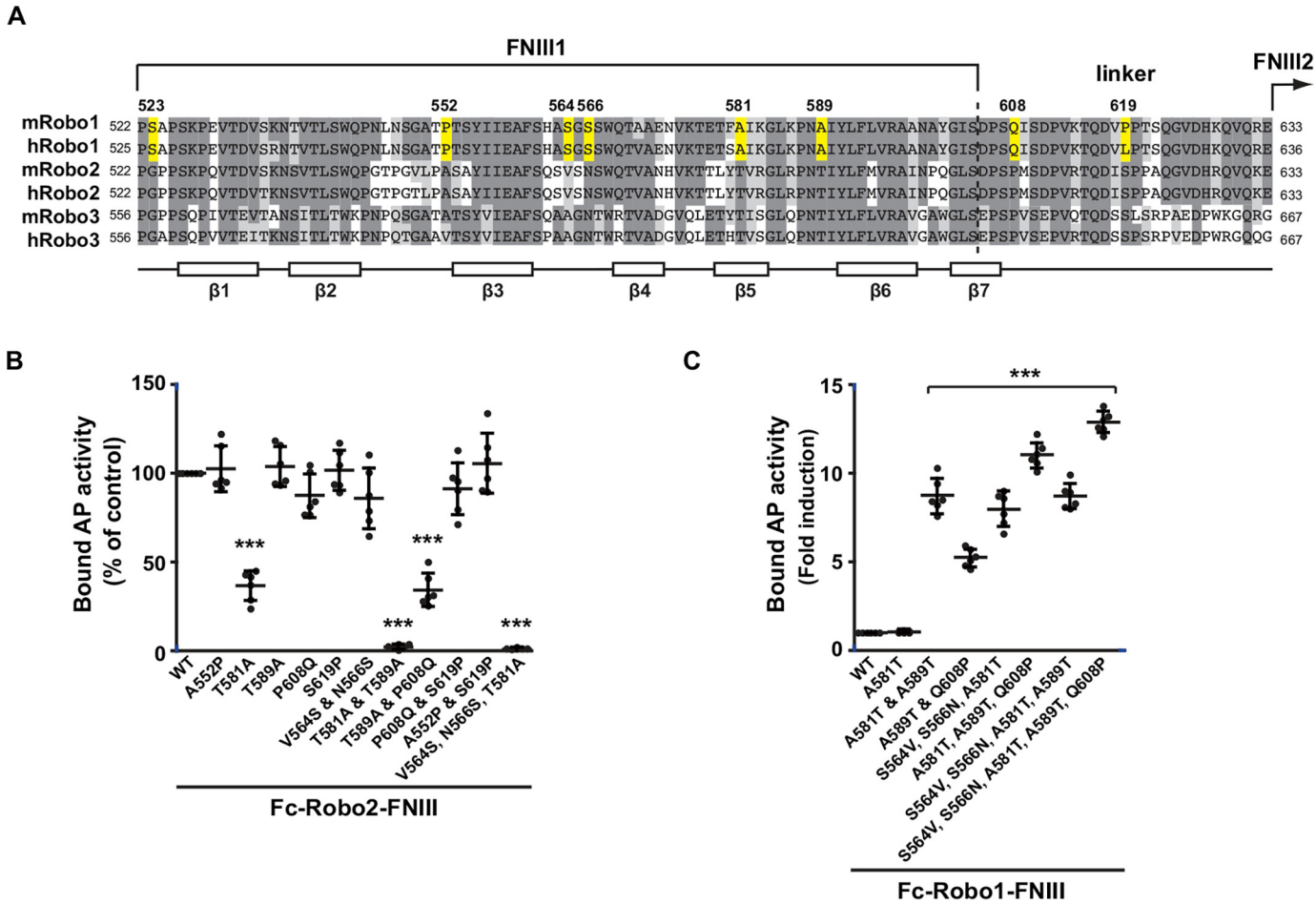

Figure 3. Identification of critical amino acids for NELL1 binding in the first FNIII domain of Robo2. *A*, amino acids sequence alignment of the first FNIII domain and linker sequence of mouse and human Robo1–3. The sequences were aligned using the program ClustalW 1.83 version (43). Identical and similar residues are *shaded* in *dark* and *light gray*, respectively. The Robo1 amino acids that are different from Robo2/3 are highlighted in *yellow*. The *boxes* below the alignment show the putative secondary structure. *B* and *C*, NELL1-binding activities of the Fc-tagged Robo2 (*B*) or Robo1 (*C*) mutants. Conditioned medium of Fc-tagged FNIII domains of Robo1/2 and their mutants were allowed to bind to protein A–coated plates and then incubated with conditioned medium of AP-tagged NELL1. The bound AP activity was measured by adding the AP substrate. Each value represents the mean ± S.D. of triplicate results ($n = 6$). ***, $p < 0.001$ when compared with the control determined by one-way analysis of variance followed by Dunnett's post hoc test.

A581T mutation showed no significant induction, double to quintuple mutants exhibited 5–13-fold induction of NELL1-binding activity. These results reinforce the above suggestion that several amino acids including Thr^{581} of mRobo2 contribute to the NELL1 binding.

A three-dimensional structure of the first FNIII domain of Robo2 was modeled using the crystal structure of the eighth FNIII domain of human sidekick 2 (Fig. S7*A*). Subsequently, the structural model of the T581A mutant was constructed based on the WT model. Analysis of the electrostatic surface potential of these homology-based structural models revealed that positively and negatively charged patches on the surface were absent in the T581A mutant probably because of conformational changes (Fig. S7, *B* and *C*), suggesting that NELL1 may interact with Robo2 through these charged patches. However, mutation of charged amino acids (Asp^{532} and Arg^{583}) in these patches did not affect NELL1-binding activity (Fig. S7*D*), suggesting that another mechanism is involved in the reduction of NELL1-binding activity of the T581A mutant.

Interaction of NELL1/2 with cell surface Robo2

To investigate whether NELL1 interacts with membrane-bound Robo2, COS1 cells were transiently transfected with the full-length Robo2 expression plasmid and its N-terminal deletion mutants (Fig. 4*A* and Fig. S8). The cells were incubated with AP-tagged NELL1, and bound NELL1 was assessed by *in situ* staining. Consistent with the results of the cell-free binding assays, AP-NELL1 showed moderate staining of cells expressing intact Robo3 but showed minimal staining of cells expressing intact Robo2 (Fig. 4*B*). However, when the first four Ig domains of Robo2 were deleted, AP-NELL1 showed significant staining. Similar results were obtained using AP-NELL2. These results suggest that the N-terminal Ig domains prevent NELL proteins from binding to the FNIII domain of Robo2.

Interaction of NELL1 with chimeric Robo2/3-ECD proteins

We prepared chimeric Robo2/3-ECD constructs by domain swapping between Ig domains and FNIII domains to investigate whether Ig domains of Robo2 have inhibitory properties on NELL1 binding. NELL1-binding activity in the solution-bind-

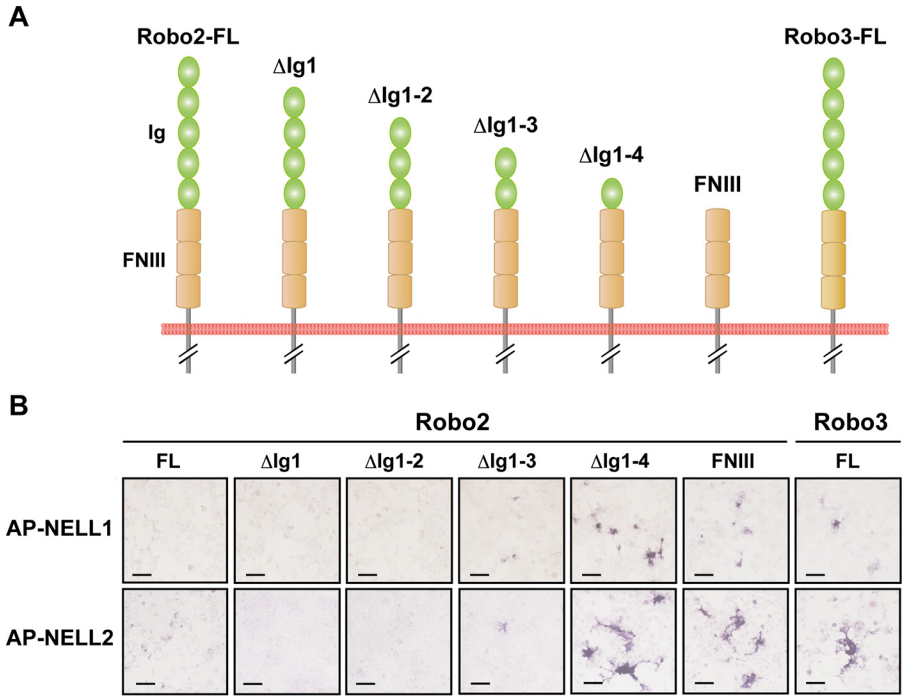

Figure 4. NELL1/2 binds to cell-surface Robo2 mutants. *A*, schematic diagrams of the Robo2 protein and its N-terminal deletion mutants. *B*, COS1 cells were transiently transfected with a series of expression plasmids and incubated with conditioned medium of AP-tagged NELL1 or NELL2. The bound AP was visualized by *in situ* staining with BCIP/NBT. The *scale bar* indicates 100 μm.

ing assay showed that both chimeric proteins were able to interact with NELL1 (Fig. 5), suggesting that NELL1 is not able to interact with intact Robo2 probably not because of the properties of the Ig domain, but because of the conformation of the entire extracellular domain structure. Interestingly, Ig domains of Robo2 bind to FNIII domains of Robo2 but not to those of Robo3 in the solid-phase binding assay (Fig. S9). This result suggests that Ig domains may mask the binding site for NELL1 by binding to FNIII domains (to be discussed later); however, the interaction between Ig domains and FNIII domains of Robo2 could not be detected in the solution-binding assay under our assay conditions (data not shown).

Amino acid substitution at the position of the predicted dimerization interface enables NELL1 to bind to the Robo2-ECD protein

Robo family members have been shown previously to interact homomerically and exist predominantly as homodimers (22, 23). Additionally, the fourth Ig (Ig4) domain of Robo2 was identified as a dimerization domain (24). NELL proteins did not bind to intact Robo2 and its deletion mutants containing the Ig4 domain (Fig. 4), prompting us to investigate whether the oligomeric state of Robo2 affects the interaction with NELL proteins. Thus, we prepared two single amino acid substitution mutants (F357R and L394R) where the hydrophobic core residues at the dimerization interface were substituted with arginine to reduce dimerization propensity (24) and tested the binding activity to NELL1 in the cell-free binding assays. As shown in Fig. 6*A*, WT Robo2-ECD did not interact with NELL1, whereas F357R or L394R mutants of Robo2-ECD co-immunoprecipitated with NELL1 in the solution-binding assay. Similar results were obtained in the solid-phase binding assay (Fig. 6*B* and Fig. S10).

To exclude the possibility that F357R and L394R mutants are prone to degradation and result in exposure of the binding site for NELL1, we confirmed these results by using purified proteins and verified the quality of the purified proteins by silver staining of SDS-polyacrylamide gels (Fig. S11). Fc-tagged Robo2-ECD proteins showed some degradation, but no such difference was observed between WT and mutants (Fig. S11*C*). We next determined the oligomeric state of the HA-tagged Robo2-ECD proteins by size-exclusion chromatography (SEC), because the Fc tag itself mediates artificial dimerization. The SEC profile of the WT Robo2-ECD revealed that most of this protein exists as a dimer (Fig. S12*A*). Unexpectedly, the L394R mutant of Robo2-ECD also exists as a dimer (Fig. S12*B*), suggesting that either the F357R or L394R substitution did not affect the oligomeric state of the Robo2-ECD but may affect the conformation of Ig domains to expose the binding site for NELL1.

Acidic conditions enable NELL1 to bind to the Robo2-ECD protein

We performed the solid-phase binding assay under acidic conditions to investigate whether low pH affects the NELL1-binding activity to the Robo2-ECD protein. As shown in Fig. 7*A*, the NELL1-binding activity increased as the pH decreased from 7.0 to 5.5, whereas the NELL1-binding activity to Robo2-FNIII did not change between pH 7.0 and 5.5 (Fig. 7*B*). These results suggest that acidic pH affects the conformation of the Ig domains but not the conformation of the FNIII domains. Similar to the Robo2-ECD, the NELL1-binding activity to the

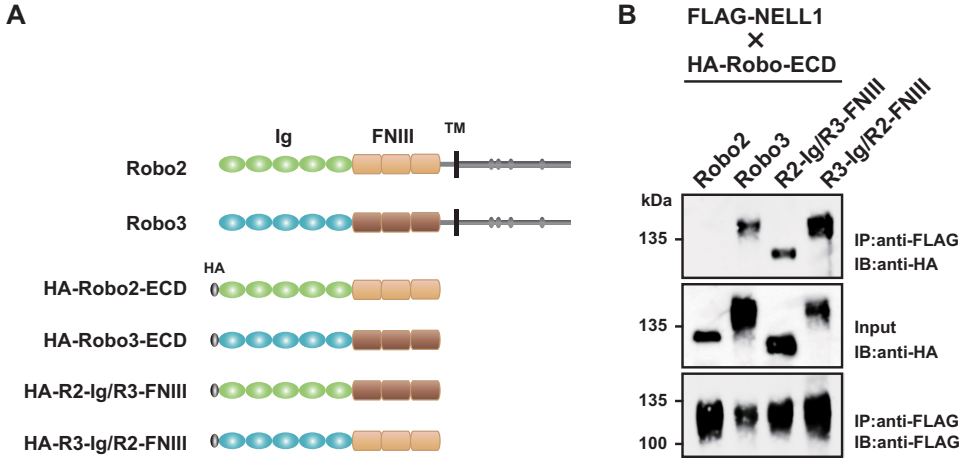

Figure 5. Interaction of NELL1 with the chimeric Robo2/3-ECD in the solution-binding assay. *A*, schematic diagrams of Robo2/3-ECD and their Ig domain-swapped mutants. *B*, conditioned media of FLAG-tagged NELL1 and HA-tagged Robo2/3-ECD were mixed and then incubated with anti-FLAG affinity beads. Bound proteins were isolated by immunoprecipitation, resolved by SDS-PAGE, and visualized by immunoblotting (*IB*) with the anti-HA antibody.

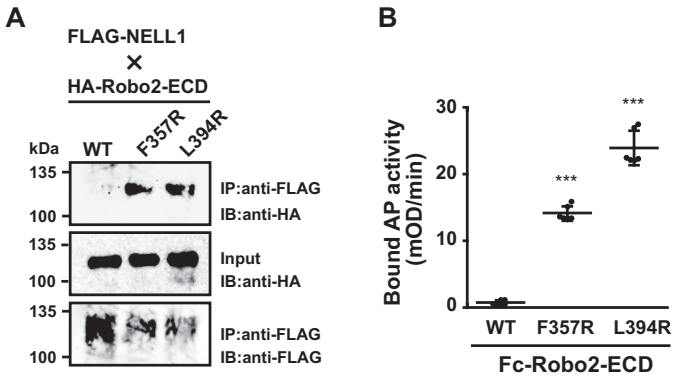

Figure 6. Amino acid substitution at the position of the predicted dimerization interface enables NELL1 to bind to the Robo2-ECD. *A* and *B*, interaction of NELL1 with the Robo2-ECD and its F357R and L394R mutants in the solution-binding assay (*A*) and the solid-phase binding assay (*B*). Each value represents the mean ± S.D. of triplicate results ($n = 6$). ***, $p < 0.001$ when compared with the control determined by one-way analysis of variance followed by Dunnett's post hoc test. *IB*, immunoblotting.

Robo3-ECD also increased as the pH decreased from 7.0 to 5.5 (Fig. 7*C*), indicating that Robo3-ECD has similar properties against acidic pH as Robo2-ECD. Acidic conditions also increased the NELL1-binding activity in cells expressing full-length Robo2 (Fig. 7*D*).

Discussion

We have investigated the binding activity of NELL1/2 to the Robo family of receptors using both cell-free and cell-based binding assays, and NELL1/2 was found to interact with not only intact Robo3 but also the Ig domain-deleted Robo2. Jaworski *et al.* (21) demonstrated that Robo3 binds to both NELL1 and NELL2; however, NELL1 is not expressed in the spinal cord at the time of commissural axon growth to the midline and has no significant effect on commissural axon repulsion *in vitro*, suggesting that NELL1 is not a functional ligand for Robo3 in commissural axons. It remains possible, however, that NELL1 functions as a ligand for Robo3 at another spatiotemporal location. For example, NELL1-deficient mice show skeletal defects with alteration of spinal curvature that may resemble the scoliosis phenotype of human patients with horizontal gaze palsy with the progressive scoliosis disorder that is caused by a mutation in the Robo3 gene (8, 25). In contrast to the skeletal defects in the vertebral column, craniofacial defects of NELL1-deficient mice indicate a deficiency of neural crest cell derivatives (6). Recently, Li *et al.* (26) demonstrated that Robo1 and Robo2 double knockout mouse embryos show the defect of cranial osteogenesis because production of cranial neural crest cells is reduced. The overlapping phenotypes of NELL1-deficient mice and Robo1/2 double knockout mice suggest that they function in a common pathway.

Robo receptors and their Slit ligands form one of the most crucial ligand–receptor pairings among axon guidance molecules. However, Slit/Robo signaling not only functions in axon guidance but also in a variety of developmental events outside the nervous system (26). For example, Slit/Robo signaling is involved in many aspects of heart development, such as cardiac cell migration and alignment (27). Recently, Kim *et al.* (28) identified osteoclast-derived Slit3 as a new coupling factor for bone resorption to bone formation and demonstrated that Slit3 stimulates osteoblastic migration and proliferation via Robo1 and Robo2 receptors in osteoblasts. They also showed that Robo1 and Robo2 are predominantly expressed in mouse calvaria osteoblasts and participate in bone formation. Although at present we have no direct evidence that NELL1 interacts with intact Robo2 *in vivo*, NELL1 may transduce a signal through Robo2 in some conditions during craniofacial bone development. Further investigation is clearly necessary to elucidate the function of the NELL1–Robo2 interaction.

Some extracellular proteins contain cryptic ligand-binding sites that have the potential to bind to ligands but are prevented from doing so under normal conditions (29, 30). Proteolytic cleavage and/or conformational changes unmask cryptic sites and expose fragments with biological activities that are not observed in the intact molecule. In this study, we have identified a cryptic binding site for NELL1/2 in the extracellular domain of Robo2. A previous reported showed that Robo1-ECD is cleaved by metalloproteinase in cancer cells, although it does not unmask a cryptic site (31). Currently, there is no study reporting the cleavage of Robo2-ECD, and a cleaved product

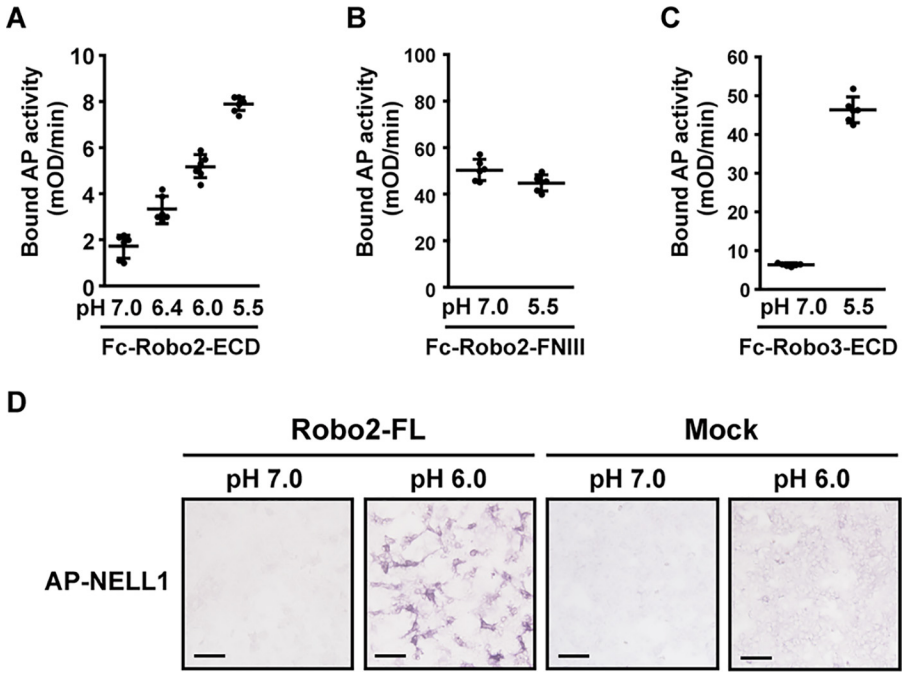

Figure 7. Acidic conditions enable NELL1 to bind to the Robo2-ECD. *A–C*, interaction between NELL1 and Robo proteins at the indicated pH values in the solid-phase binding assay. Purified protein of Robo2-ECD (*A*), Robo2-FNIII (*B*), or Robo3-ECD (*C*) was allowed to bind to protein A– coated plates and then incubated with purified protein of AP-tagged NELL1-C. The bound AP activity was measured by adding the AP substrate. Each value represents the mean ± S.D. of triplicate results ($n = 6$). *D*, COS1 cells were transiently transfected with an expression plasmid for Robo2-FL and incubated with conditioned medium of AP-tagged NELL1. The bound AP was visualized by *in situ* staining with BCIP/NBT. The *scale bar* indicates 100 μm.

was not found in the cells, as far as we examined (data not shown). A database search also indicates that there are no alternative splicing products that correspond to Ig domain-deficient Robo2. If proteolytic cleavage has not occurred, conformational changes to the extracellular domains of Robo2 may be possible mechanisms of NELL1/2–Robo2 interaction.

Formerly, ligand-induced receptor dimerization was the proposed mechanism for activation of most transmembrane receptors. However, recent studies suggest that various transmembrane receptors exist as preformed, yet inactive, dimers on the cell surface, and then ligand binding to the preformed dimers induces activation of intracellular domains (32). Robo family receptors have been shown to participate in homomeric interactions on the cell surface and exist predominantly as homodimers in the basal state (22, 23). Yom-Tov *et al.* (24) identified that Ig4 is a Robo dimerization domain, and two amino acid residues, Phe^{357} and Leu^{394}, in the Ig4 domain of Robo2 are important for dimerization. Interestingly, single amino acid substitution mutants (F357R or L394R) that reduce the dimerization propensity of the Ig4 domain showed the strong binding to NELL1. However, our SEC analysis of the L394R mutant of the Robo2-ECD protein indicated that the L394R substitution did not affect the dimerization propensity. This is probably because the protein domain used in this assay and that used by the Yom-Tov's group differ; they used Ig domains only, whereas we used the whole extracellular domain. Although the oligomeric state of Robo2 may not be important for NELL1 binding, the results from the binding experiments of F357R and L394R mutants suggest that conformational changes to the extracellular domain of Robo2 unmask the cryptic fragment in the first FNIII domain that interacts with NELL1. The results of the domain-swapping experiment may support this implication (Fig. 5).

Extracellular acidification has been observed under many pathological conditions, such as ischemia, inflammation, and tumor progression (33). Metabolic acidosis causes a decrease in bone mineral density by causing cell death of osteoblasts and the activation of osteoclasts to resorb bone (34). In this study, we have identified a pH-dependent interaction between NELL1 and Robo2. We hypothesize that the NELL1-binding site of Robo2 is masked by Ig domains at neutral pH but is exposed under acidic pH conditions by conformational changes to the ectodomain (Fig. 8). We showed that Ig domains of Robo2 can bind to FNIII domains in the solid-phase binding assay, and this interaction was enhanced under acidic pH conditions (Fig. S9). This appears inconsistent with our hypothesis; however, those binding experiments were performed using the fragment of each domain. Although further studies using the intact ectodomain are required to determine whether the Ig domains can bind to the FNIII domains, the interaction between NELL1 and Robo2 in osteoblasts under acidic conditions may enhance bone formation to recover bone mass.

Slit proteins, major ligands for Robo1 and Robo2, bind to the first Ig (Ig1) domain of Robo receptors to initiate cell signaling (35), whereas mammalian Robo3 has lost the ability to bind Slit proteins because of a few amino acid changes in its Ig1 domain (20). Because the cytosolic domains of Robo receptors are catalytically inactive, it is thought that several catalytically active molecules or inactive adaptors bind to cytosolic domains of Robo, and these interactions are somehow regulated by Slit proteins (17). Jaworski *et al.* (21) showed that NELL2 binds to Robo3 and serves indirectly as a negative regulator of Slit sig-

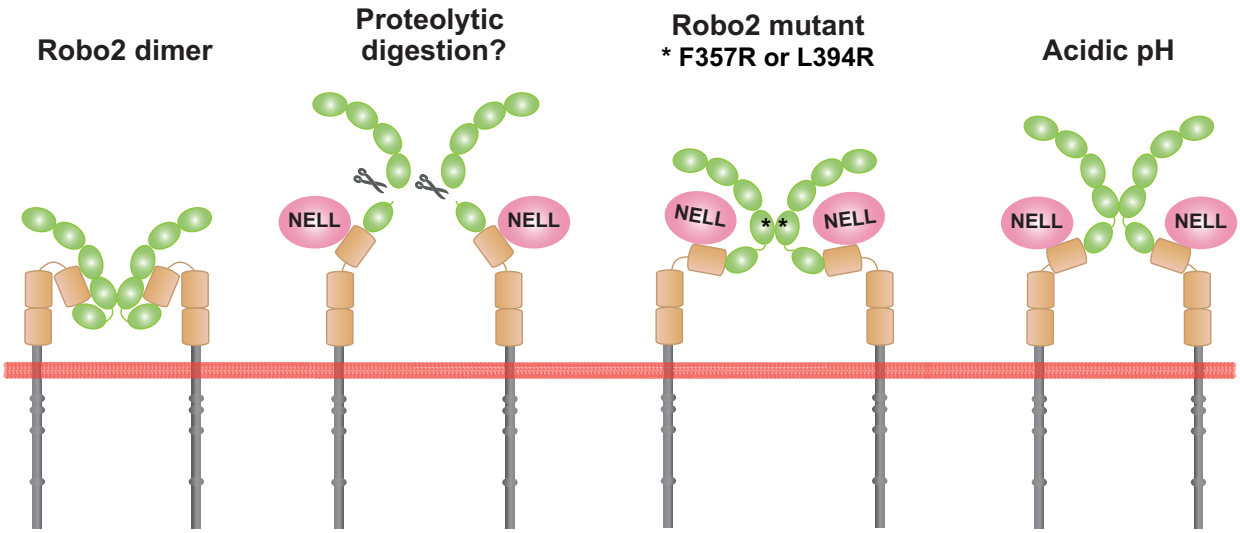

Figure 8. Summary of possible interactions between Robo2 and NELL proteins.

naling; however, no signaling pathway downstream of the NELL2-Robo3 interaction has been identified. We preliminarily examined the signaling pathway downstream of the NELL1-Robo2 interaction in osteoblastic cells; however, no clear results were obtained. It is essential to continue to investigate the downstream signaling events involved in interaction between NELL1 and Robo2.

In summary, our comprehensive analysis of NELL–Robo interactions demonstrated that Robo2 contains a cryptic binding site for NELL1/2 within the first FNIII domain. Mutation analysis revealed that the difference of several amino acids is responsible for the NELL1-binding activity among the Robo family of receptors. Furthermore, our data suggest that conformational changes of the ectodomain of Robo2 unmask the binding site for NELL1/2. Although the role of NELL1/2–Robo2 interactions remains unknown, the findings of our current study may provide useful information on potential novel signaling pathways triggered by NELL1/2.

Experimental procedures

Antibodies

Mouse monoclonal antibodies against FLAG (Sigma–Aldrich), HA (Medical & Biological Laboratories (MBL), Nagoya, Japan), and c-Myc (Santa Cruz Biotechnology, Santa Cruz, CA) epitopes were purchased from the indicated manufacturers. Horseradish peroxidase–conjugated anti-mouse and anti-human IgGs were purchased from GE Healthcare.

Plasmid construction

An expression vector for full-length human NELL1 with an N-terminal FLAG tag was prepared as described previously (36) and designated FLAG-NELL1. An expression vector for full-length mouse NELL2 with an N-terminal FLAG tag was prepared as follows: cDNA encoding the mouse NELL2 (residues 25–819) was amplified by RT-PCR from total RNA isolated from mouse brain. The PCR product was digested with appropriate restriction enzymes, cloned into the pSecTag2-FLAG vector (37), and designated FLAG-NELL2. Expression vectors for full-length human NELL1 and NELL2 with an N-terminal AP tag were prepared as follows: cDNA encoding the human NELL1 (residues 17–810) or human NELL2 (residues 22–816) were amplified by RT-PCR from total RNA isolated from human brain (Invitrogen). The PCR products were digested with appropriate restriction enzymes, cloned into the pAPtag-5 vector (GenHunter, Nashville, TN), and designated AP-NELL1 or AP-NELL2. An expression vector for the C-terminal region (residues 273–810) of human NELL1 with an N-terminal AP tag was prepared as described previously (38) and designated AP-NELL1-C. cDNA fragments encoding the deletion mutants of EGFL domains of human NELL1 (residues 389–517, 479–595, 389–478, 434–517, and 479–517) were amplified by PCR using a full-length NELL1 cDNA as the template, cloned into the pAPtag-5 vector, and designated AP-NELL1-EGFL123, AP-NELL1-EGFL345, AP-NELL1-EGFL12, AP-NELL1-EGFL23, and AP-NELL1-EGFL3, respectively. The domain structures were predicted by the simple molecular architecture research tool (SMART) program (http://smart.embl.de)[3] (39–41). An expression vector for Ig1–5 domains of mouse Robo2 with a C-terminal AP tag was prepared as follows: cDNA encoding the mouse Robo2 (residues 22–513) was amplified by RT-PCR from total RNA isolated from mouse brain. The PCR products were digested with appropriate restriction enzymes, cloned into the pAPtag-5 vector, and designated AP-Robo2-Ig.

Expression vectors for ECDs or FNIII domains of mouse Robo1–4 (GenBank™ database accession nos. NP_062286.2, NP_780758.3, NP_001158239.1, and NP_001296319.1) with an N-terminal HA tag were prepared as follows: cDNAs encoding the mouse Robo1 (residues 20–858 or 525–858), mouse Robo2 (residues 22–875 or 522–859), mouse Robo3 (residues 21–891 or 556–891), and mouse Robo4 (residues 38–479 or 263–479) were amplified by RT-PCR from total RNA isolated from mouse brain. The PCR products were digested with appropriate restriction enzymes, cloned into the pSecTag2-HA vector, and designated HA-Robo-ECD and HA-Robo-FNIII, respectively. pSecTag2-HA was generated by subcloning annealed oligonu-

[3] Please note that the JBC is not responsible for the long-term archiving and maintenance of this site or any other third party hosted site.

cleotides encoding the HA epitope (YPYDVPDYA) into the HindIII–BamHI sites of the pSecTag2A mammalian expression vector (Invitrogen). For domain-swapping constructs, amplicons were inserted using the In-Fusion HD cloning kit (Takara Bio, Otsu, Japan).

Expression vectors for full-length mouse Robo2 and Robo3 with a C-terminal HA tag were prepared as follows: full-length cDNAs encoding the mouse Robo2 (residues 1–1508) and Robo3 (residues 1–1402) were amplified by RT-PCR from total RNA isolated from mouse brain. The PCR products were digested with appropriate restriction enzymes, cloned into the pcDNA3.1-HA vector, and designated Robo2-FL and Robo3-FL. pcDNA3.1-HA was generated by subcloning annealed oligonucleotides encoding the HA epitope into the XbaI–AgeI sites of the pcDNA3.1/*myc*-HisA mammalian expression vector (Invitrogen). Deletion mutants of the full-length Robo2 expression plasmid lacking the coding sequence for the part of five Ig domains (residues 43–144, 43–236, 43–323, 43–429, and 43–521) were generated by inverse PCR and designated Robo2-ΔIg1, Robo2-ΔIg1–2, Robo2-ΔIg1–3, Robo2-ΔIg1–4, and Robo2-FNIII, respectively.

Expression vectors for ECD or FNIII domains of mouse Robo1–4 with a C-terminal human immunoglobulin Fc tag were prepared similarly except that the PCR products were cloned into the pFUSE-hIgG1-Fc2 vector (Invivogen, San Diego, CA), and designated Fc-Robo-ECD and Fc-Robo-FNIII. cDNA fragments encoding the deletion mutants of FNIII domains of mouse Robo2 (residues 522–635 and 636–859) were amplified by PCR using a Robo2 cDNA as a template, cloned into the pFUSE-hIgG1-Fc2 vector, and designated Fc-Robo2-FNIII1 and Fc-Robo2-FNIII23, respectively. cDNA fragments encoding the deletion mutants of FNIII domains of mouse Robo3 (residues 556–669 and 671–891) were amplified by PCR using Robo3 cDNA as a template, cloned into the pFUSE-hIgG1-Fc2 vector, and designated Fc-Robo3-FNIII1 and Fc-Robo3-FNIII23, respectively. The amino acid substitution mutants were generated by site-directed mutagenesis using inverse PCR.

Protein expression and purification

Recombinant NELL and Robo proteins were produced by the FreeStyle MAX 293 expression system (Invitrogen), according to the manufacturer's instructions. Briefly, 293-F cells were transfected with the expression plasmids using the FreeStyle MAX reagent (Invitrogen) and grown in serum-free FreeStyle 293 expression medium (Invitrogen) for 1–4 days. When necessary, recombinant proteins with hexahistidine tag were purified from the conditioned media using 1-ml HisTrap HP columns (GE Healthcare) as described previously (42). For purification of recombinant proteins with Fc tag, conditioned media were applied to 1-ml HiTrap protein A HP columns (GE Healthcare) and then washed with binding buffer (20 mM sodium phosphate, pH 7.0). Bound proteins were eluted with 0.1 M citric acid, pH 3.0, and neutralized with 15% (v/v) of 1 M Tris-HCl, pH 9.0. If necessary, recombinant proteins were concentrated using a Vivaspin 6 (10-kDa molecular mass cutoff; GE Healthcare). Purified proteins were analyzed by SDS-PAGE (SDS-PAGE) under reducing conditions, and separated proteins were visualized by Coomassie Brilliant Blue R-250 staining (Quick-CBB; Wako, Osaka, Japan) or silver staining (EzStain Silver; Atto, Tokyo, Japan).

Cell-free binding assay

Solution-binding assays were performed as follows: conditioned media or purified proteins of HA-Robo and FLAG-NELL1 were incubated at 4 °C for 1 h, and the complex was immunoprecipitated with anti-FLAG M2 affinity beads (Sigma–Aldrich) at 4 °C for 1 h. The beads were washed three times with HBAH buffer (0.2% BSA, and 20 mM HEPES, pH 7.0, in Hanks' balanced salt solution), and the complex was eluted with 150 μg/ml FLAG peptide (Sigma–Aldrich). The eluted samples were separated on SDS-polyacrylamide gels and immunoblotted with the anti-HA antibody.

Solid-phase binding assays were performed using Reacti-Bind protein A–coated plates (Thermo Scientific, Waltham, MA). Wells were blocked with HBAH buffer for 15 min. Conditioned media or purified proteins of Fc-Robo were allowed to bind to protein A for 90 min at room temperature. The wells were washed four times with HBAH buffer, treated with conditioned media of AP-tagged proteins or purified protein of AP-NELL1-C for 90 min at room temperature, and then washed four times with HBAH buffer. When analyzed under acidic conditions, AP-tagged proteins were incubated in 0.1 M MES buffer (pH range 5.5–6.4). The bound AP activity (absorbance at 405 nm/min) was measured using the alkaline phosphatase yellow (paranitrophenylphosphate) liquid substrate system (Sigma–Aldrich).

Immunoblot analysis

Proteins were separated on SDS-polyacrylamide gels, followed by transfer onto Amersham Biosciences Protran Premium 0.45 nitrocellulose membranes (GE Healthcare). The membranes were blocked with 5% (w/v) skim milk in PBS containing 0.1% (v/v) Tween 20, followed by incubation with the primary antibody for 1 h at room temperature. The membranes were then washed and incubated with the horseradish peroxidase–conjugated secondary antibody for 1 h at room temperature. The membranes were developed with the ECL start Western blotting detection reagent (GE Healthcare) and imaged on an LAS-4000mini luminescent image analyzer (GE Healthcare).

Cell surface–binding assay

Monkey kidney COS1 cells were maintained in Dulbecco's modified Eagle's medium containing 10% (v/v) fetal calf serum. Transient transfection of COS1 cells was carried out using the FuGENE HD transfection reagent (Promega, Madison, WI), according to the manufacturer's instructions. Transiently transfected COS1 cells were incubated with the conditioned media of AP-NELL1 or AP-NELL2 (~2 nM) for 90 min at room temperature. When analyzed under acidic conditions, conditioned media were adjusted to pH 6.0 with HCl. The cells were washed three times with the HBAH buffer and fixed in 4% paraformaldehyde for 15 min. Fixed cells were washed three times with 20 mM HEPES, pH 7.0, 150 mM NaCl, incubated at 65 °C for 100 min to inactivate endogenous AP, washed with AP

buffer (100 mM Tris-HCl, pH 9.0, 150 mM NaCl, 1 mM $MgCl_2$) and stained with the 5-bromo-4-chloro-3-indolyl-phosphate (BCIP)/nitroblue tetrazolium (NBT) solution kit (Nakalai Tesque, Kyoto, Japan) at room temperature overnight.

Biolayer interferometry analysis

The binding properties of NELL1 and Robo2 were analyzed by biolayer interferometry by using BLItz system (Pall ForteBio, Menlo Park, CA). The purified full-length human NELL1 protein was biotinylated using a biotin labeling kit-NH_2 (Dojindo Molecular Technologies, Kumamoto, Japan) and immobilized on a streptavidin sensor for 120 s in WS buffer (Dojindo Molecular Technologies). Subsequently, we measured the association (120 s) of 4 μl of purified FNIII domains of Robo2 at various concentrations (1, 2, and 4 μM) in kinetics buffer (Pall ForteBio) and their dissociation (120 s) in 400 μl of Kinetics Buffer. Data analysis was performed with BLItzPro software (version 1.2.1.3, Pall ForteBio). A 1:1 binding model was employed to fit the data.

Homology modeling

Homology models for the first FNIII domain of mouse Robo2 were generated by the Molecular Operating Environment software package (version 2018.01; Chemical Computing Group, Montreal, Canada). The crystal structure of the eighth FNIII domain of human sidekick-2 (Protein Data Bank code 1WFO.A) was used as the structural template. The structure of the T581A mutant was built using the Molecular Operating Environment protein builder function.

Size-exclusion chromatography

The purified proteins (~100 μg) were analyzed by size-exclusion chromatography on a HiPrep 16/60 Sephacryl S-300 HR column (GE Healthcare) in 50 mM sodium phosphate buffer, pH 7.4, containing 150 mM NaCl using an AKTAprime plus system (GE Healthcare). The column was calibrated with a gel filtration calibration kit HMW (GE Healthcare).

Author contributions—N. Y., M. K., M. I., T. K., and T. N. investigation; T. K. and T. N. methodology; T. K., A. D. M., S. K., and T. N. writing-review and editing; A. D. M., S. K., and T. N. resources; S. K. and T. N. supervision; T. N. conceptualization; T. N. data curation; T. N. formal analysis; T. N. funding acquisition; T. N. validation; T. N. visualization; T. N. writing-original draft; T. N. project administration.

Acknowledgment—We thank Edanz Group for editing a draft of this manuscript.

References

1. Watanabe, T. K., Katagiri, T., Suzuki, M., Shimizu, F., Fujiwara, T., Kanemoto, N., Nakamura, Y., Hirai, Y., Maekawa, H., and Takahashi, E. (1996) Cloning and characterization of two novel human cDNAs (NELL1 and NELL2) encoding proteins with six EGF-like repeats. *Genomics* **38,** 273–276 CrossRef Medline
2. Kuroda, S., Oyasu, M., Kawakami, M., Kanayama, N., Tanizawa, K., Saito, N., Abe, T., Matsuhashi, S., and Ting, K. (1999) Biochemical characterization and expression analysis of neural thrombospondin-1-like proteins NELL1 and NELL2. *Biochem. Biophys. Res. Commun.* **265,** 79–86 CrossRef Medline
3. Aihara, K., Kuroda, S., Kanayama, N., Matsuyama, S., Tanizawa, K., and Horie, M. (2003) A neuron-specific EGF family protein, NELL2, promotes survival of neurons through mitogen-activated protein kinases. *Brain Res. Mol. Brain Res.* **116,** 86–93 CrossRef Medline
4. Nelson, B. R., Claes, K., Todd, V., Chaverra, M., and Lefcort, F. (2004) NELL2 promotes motor and sensory neuron differentiation and stimulates mitogenesis in DRG *in vivo*. *Dev. Biol.* **270,** 322–335 CrossRef Medline
5. Zhang, X., Zara, J., Siu, R. K., Ting, K., and Soo, C. (2010) The role of NELL-1, a growth factor associated with craniosynostosis, in promoting bone regeneration. *J. Dent. Res.* **89,** 865–878 CrossRef Medline
6. Ting, K., Vastardis, H., Mulliken, J. B., Soo, C., Tieu, A., Do, H., Kwong, E., Bertolami, C. N., Kawamoto, H., Kuroda, S., and Longaker, M. T. (1999) Human NELL-1 expressed in unilateral coronal synostosis. *J. Bone Miner. Res.* **14,** 80–89 CrossRef Medline
7. Zhang, X., Kuroda, S., Carpenter, D., Nishimura, I., Soo, C., Moats, R., Iida, K., Wisner, E., Hu, F. Y., Miao, S., Beanes, S., Dang, C., Vastardis, H., Longaker, M., Tanizawa, K., *et al.* (2002) Craniosynostosis in transgenic mice overexpressing Nell-1. *J. Clin. Invest.* **110,** 861–870 CrossRef Medline
8. Desai, J., Shannon, M. E., Johnson, M. D., Ruff, D. W., Hughes, L. A., Kerley, M. K., Carpenter, D. A., Johnson, D. K., Rinchik, E. M., and Culiat, C. T. (2006) Nell1-deficient mice have reduced expression of extracellular matrix proteins causing cranial and vertebral defects. *Hum. Mol. Genet.* **15,** 1329–1341 CrossRef Medline
9. Zhang, X., Ting, K., Pathmanathan, D., Ko, T., Chen, W., Chen, F., Lee, H., James, A. W., Siu, R. K., Shen, J., Culiat, C. T., and Soo, C. (2012) Calvarial cleidocraniodysplasia-like defects with ENU-induced Nell-1 deficiency. *J. Craniofac. Surg.* **23,** 61–66 CrossRef Medline
10. Bokui, N., Otani, T., Igarashi, K., Kaku, J., Oda, M., Nagaoka, T., Seno, M., Tatematsu, K., Okajima, T., Matsuzaki, T., Ting, K., Tanizawa, K., and Kuroda, S. (2008) Involvement of MAPK signaling molecules and Runx2 in the NELL1-induced osteoblastic differentiation. *FEBS Lett.* **582,** 365–371 CrossRef Medline
11. Shen, J., James, A. W., Chung, J., Lee, K., Zhang, J. B., Ho, S., Lee, K. S., Kim, T. M., Niimi, T., Kuroda, S., Ting, K., and Soo, C. (2012) NELL-1 promotes cell adhesion and differentiation via integrin β1. *J. Cell. Biochem.* **113,** 3620–3628 CrossRef Medline
12. James, A. W., Shen, J., Zhang, X., Asatrian, G., Goyal, R., Kwak, J. H., Jiang, L., Bengs, B., Culiat, C. T., Turner, A. S., Seim Iii, H. B., Wu, B. M., Lyons, K., Adams, J. S., Ting, K., *et al.* (2015) NELL-1 in the treatment of osteoporotic bone loss. *Nat. Commun.* **6,** 7362 CrossRef Medline
13. Li, C. S., Zhang, X., Péault, B., Jiang, J., Ting, K., Soo, C., and Zhou, Y. H. (2016) Accelerated chondrogenic differentiation of human perivascular stem cells with NELL-1. *Tissue Eng. Part A* **22,** 272–285 CrossRef Medline
14. Li, C., Jiang, J., Zheng, Z., Lee, K. S., Zhou, Y., Chen, E., Culiat, C. T., Qiao, Y., Chen, X., Ting, K., Zhang, X., and Soo, C. (2017) Neural EGFL-like 1 is a downstream regulator of runt-related transcription factor 2 in chondrogenic differentiation and maturation. *Am. J. Pathol.* **187,** 963–972 CrossRef Medline
15. Li, C., Zheng, Z., Jiang, J., Jiang, W., Lee, K., Berthiaume, E. A., Chen, E. C., Culiat, C. T., Zhou, Y. H., Zhang, X., Ting, K., and Soo, C. (2018) Neural EGFL-like 1 regulates cartilage maturation through runt-related transcription factor 3-mediated Indian hedgehog signaling. *Am. J. Pathol.* **188,** 392–403 CrossRef Medline
16. Patel, B. N., and Van Vactor, D. L. (2002) Axon guidance: the cytoplasmic tail. *Curr. Opin. Cell Biol.* **14,** 221–229 CrossRef Medline
17. Hohenester, E. (2008) Structural insight into Slit–Robo signalling. *Biochem. Soc. Trans.* **36,** 251–256 CrossRef Medline
18. Ballard, M. S., and Hinck, L. (2012) A roundabout way to cancer. *Adv. Cancer Res.* **114,** 187–235 CrossRef Medline
19. Ypsilanti, A. R., Zagar, Y., and Chédotal, A. (2010) Moving away from the midline: new developments for Slit and Robo. *Development* **137,** 1939–1952 CrossRef Medline
20. Seiradake, E., Jones, E. Y., and Klein, R. (2016) Structural perspectives on axon guidance. *Annu. Rev. Cell Dev. Biol.* **32,** 577–608 CrossRef Medline

21. Jaworski, A., Tom, I., Tong, R. K., Gildea, H. K., Koch, A. W., Gonzalez, L. C., and Tessier-Lavigne, M. (2015) Operational redundancy in axon guidance through the multifunctional receptor Robo3 and its ligand NELL2. *Science* **350,** 961–965 CrossRef Medline
22. Hivert, B., Liu, Z., Chuang, C.-Y., Doherty, P., and Sundaresan, V. (2002) Robo1 and Robo2 are homophilic binding molecules that promote axonal growth. *Mol. Cell. Neurosci.* **21,** 534–545 CrossRef Medline
23. Zakrys, L., Ward, R. J., Pediani, J. D., Godin, A. G., Graham, G. J., and Milligan, G. (2014) Roundabout 1 exists predominantly as a basal dimeric complex and this is unaffected by binding of the ligand Slit2. *Biochem. J.* **461,** 61–73 CrossRef Medline
24. Yom-Tov, G., Barak, R., Matalon, O., Barda-Saad, M., Guez-Haddad, J., and Opatowsky, Y. (2017) Robo Ig4 is a dimerization domain. *J. Mol. Biol.* **429,** 3606–3616 CrossRef Medline
25. Jen, J. C., Chan, W. M., Bosley, T. M., Wan, J., Carr, J. R., Rüb, U., Shattuck, D., Salamon, G., Kudo, L. C., Ou, J., Lin, D. D., Salih, M. A., Kansu, T., Al Dhalaan, H., Al Zayed, Z., *et al.* (2004) Mutations in a human ROBO gene disrupt hindbrain axon pathway crossing and morphogenesis. *Science* **304,** 1509–1513 CrossRef Medline
26. Li, Y., Zhang, X. T., Wang, X. Y., Wang, G., Chuai, M., Münsterberg, A., and Yang, X. (2017) Robo signaling regulates the production of cranial neural crest cells. *Exp. Cell Res.* **361,** 73–84 CrossRef Medline
27. Zhao, J., and Mommersteeg, M. T. M. (2018) Slit–Robo signalling in heart development. *Cardiovasc. Res.* **114,** 794–804 CrossRef Medline
28. Kim, B. J., Lee, Y. S., Lee, S. Y., Baek, W. Y., Choi, Y. J., Moon, S. A., Lee, S. H., Kim, J. E., Chang, E. J., Kim, E. Y., Yoon, J., Kim, S. W., Ryu, S. H., Lee, S. K., Lorenzo, J. A., *et al.* (2018) Osteoclast-secreted SLIT3 coordinates bone resorption and formation. *J. Clin. Invest.* **128,** 1429–1441 CrossRef Medline
29. Davis, G. E., Bayless, K. J., Davis, M. J., and Meininger, G. A. (2000) Regulation of tissue injury responses by the exposure of matricryptic sites within extracellular matrix molecules. *Am. J. Pathol.* **156,** 1489–1498 CrossRef Medline
30. Schenk, S., and Quaranta, V. (2003) Tales from the crypt[ic] sites of the extracellular matrix. *Trends Cell Biol.* **13,** 366–375 CrossRef Medline
31. Seki, M., Watanabe, A., Enomoto, S., Kawamura, T., Ito, H., Kodama, T., Hamakubo, T., and Aburatani, H. (2010) Human ROBO1 is cleaved by metalloproteinases and gamma-secretase and migrates to the nucleus in cancer cells. *FEBS Lett.* **584,** 2909–2915 CrossRef Medline
32. Maruyama, I. N. (2015) Activation of transmembrane cell-surface receptors via a common mechanism?: the "rotation model." *Bioessays* **37,** 959–967 Medline
33. Okajima, F. (2013) Regulation of inflammation by extracellular acidification and proton-sensing GPCRs. *Cell. Signal.* **25,** 2263–2271 CrossRef Medline
34. Arnett, T. R. (2010) Acidosis, hypoxia and bone. *Arch. Biochem. Biophys.* **503,** 103–109 CrossRef Medline
35. Liu, Z., Patel, K., Schmidt, H., Andrews, W., Pini, A., and Sundaresan, V. (2004) Extracellular Ig domains 1 and 2 of Robo are important for ligand (Slit) binding. *Mol. Cell. Neurosci.* **26,** 232–240 CrossRef Medline
36. Nakamura, Y., Hasebe, A., Takahashi, K., Iijima, M., Yoshimoto, N., Maturana, A. D., Ting, K., Kuroda, S., and Niimi, T. (2014) Oligomerization-induced conformational change in the C-terminal region of Nel-like molecule 1 (NELL1) protein is necessary for the efficient mediation of murine MC3T3-E1 cell adhesion and spreading. *J. Biol. Chem.* **289,** 9781–9794 CrossRef Medline
37. Phan, H. P., Sugino, M., and Niimi, T. (2009) The production of recombinant human laminin-332 in a *Leishmania tarentolae* expression system. *Protein Expr. Purif.* **68,** 79–84 CrossRef Medline
38. Takahashi, K., Imai, A., Iijima, M., Yoshimoto, N., Maturana, A. D., Kuroda, S., and Niimi, T. (2015) Mapping the heparin-binding site of the osteoinductive protein NELL1 by site-directed mutagenesis. *FEBS Lett.* **589,** 4026–4032 CrossRef Medline
39. Schultz, J., Milpetz, F., Bork, P., and Ponting, C. P. (1998) SMART, a simple modular architecture research tool: Identification of signaling domains. *Proc. Natl. Acad. Sci. U.S.A.* **95,** 5857–5864 CrossRef Medline
40. Letunic, I., Doerks, T., and Bork, P. (2015) SMART: recent updates, new developments and status in 2015. *Nucleic Acids Res.* **43,** D257–D260 CrossRef Medline
41. Letunic, I., and Bork, P. (2018) 20 years of the SMART protein domain annotation resource. *Nucleic Acids Res.* **46,** D493–D496 CrossRef Medline
42. Hasebe, A., Tashima, H., Ide, T., Iijima, M., Yoshimoto, N., Ting, K., Kuroda, S., and Niimi, T. (2012) Efficient production and characterization of recombinant human NELL1 protein in human embryonic kidney 293-F cells. *Mol. Biotechnol.* **51,** 58–66 CrossRef Medline
43. Thompson, J. D., Higgins, D. G., and Gibson, T. J. (1994) CLUSTAL W: improving the sensitivity of progressive multiple sequence alignment through sequence weighting, position-specific gap penalties and weight matrix choice. *Nucleic Acids Res.* **22,** 4673–4680 CrossRef Medline